# Using Shape Anisotropy to Toughen Disordered Nanoparticle Assemblies

**Lei Zhang,[†] Gang Feng,[‡,*] Zorana Zeravcic,[§] Teresa Brugarolas,[†] Andrea J. Liu,[⊥] and Daeyeon Lee[†,*]**

[†]Department of Chemical and Biomolecular Engineering, University of Pennsylvania, Philadelphia, Pennsylvania 19104, United States, [‡]Department of Mechanical Engineering, Villanova University, Villanova, Pennsylvania 19085, United States, [§]School of Engineering and Applied Sciences and Kavli Institute for Bionano Science and Technology, Harvard University, Cambridge, Massachusetts 02138, United States, and [⊥]Department of Physics and Astronomy, University of Pennsylvania, Philadelphia, Pennsylvania 19104, United States

**ABSTRACT** Assemblies of disordered nanoparticles constitute an important class of materials that have numerous applications in energy conversion and storage, electronics, photonics, and sensing. One major roadblock that limits the widespread utilization of disordered nanoparticle assemblies (DNAs) is their poor damage tolerance; they fracture under small loads and, thus, have low toughness. The absence of fundamental understanding on the mechanical behavior and failure mechanism of disordered nanoparticle assemblies makes it even more challenging to develop new strategies to toughen these structures without compromising their mechanical strength. Here we show the formation of shear bands, highly localized regions of mechanical strain that prelude fracture, in disordered assemblies of spherical nanoparticles, which bear striking resemblance to the deformation mechanism of a different class of disordered materials, metallic glasses. We demonstrate that anisotropic nanoparticles greatly suppress shear band formation and toughen nanoparticle packings without sacrificing their strength, implying that tuning constituent anisotropy can be used to enhance toughness in disordered packings of nanoparticles.

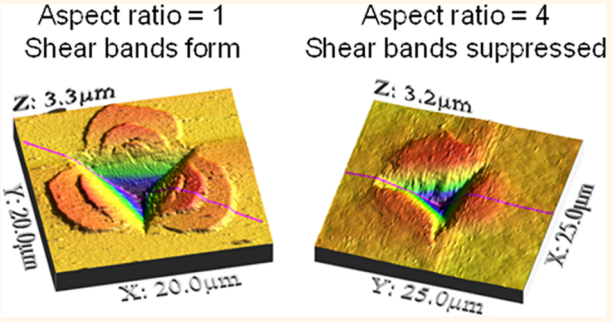


**KEYWORDS:** shape anisotropy · disordered nanoparticle assemblies · shear band · fracture toughness · nanoindentation

Disordered nanoparticle assemblies represent one of the most important classes of structures that enable the utilization of functional nanomaterials in advanced applications such as energy conversion and storage,[1,2] electronics,[3] photonics,[4,5] optics and sensing.[6] The photoanode in the dye-sensitized solar cell (DSSC), for example, is a disordered packing of $TiO_2$ nanoparticles that enable the utilization of solar energy.[1] Displays based on the colloidal films of quantum dots are another promising example of novel devices that derive their function from disordered nanoparticle assemblies (DNAs).[5] Although these DNAs are becoming increasingly important in the next generation of nanomaterial-based devices, their poor damage tolerance significantly limits their widespread utilization. DNAs permanently deform and fracture under small loads; that is, they are brittle and their toughness is very low. Conventional methods of strengthening DNAs, unfortunately, tend to make them brittle. Thus, a new strategy to generate tough and durable DNAs that will enable the fabrication of flexible energy, electronic, photonic and sensing devices is highly desirable.

Unlike highly ordered structures such as superlattices of nanoparticles,[7] the assemblies of disordered nanoparticles do not have long-range order nor do they have well-defined structural defects. The disordered structure of these nanoparticle assemblies complicates the fundamental understanding of their mechanical behavior and poses a significant challenge in developing strategies to enhance their resistance to permanent damage. A small number of studies on the mechanical behavior of DNAs have mainly focused on the assemblies made of spherical nanoparticles.[8−10] Considering the recent advances in nanomaterials chemistry, shape anisotropy presents a unique opportunity to tailor and enhance the mechanical properties of DNAs. However, surprisingly little is known about the mechanical properties of such packings, despite the fact that packing behavior of

* Address correspondence to gang.feng@villanova.edu, daeyeon@seas.upenn.edu.

Received for review June 25, 2013 and accepted August 25, 2013.

**Published online August 26, 2013**
**10.1021/nn403214p**

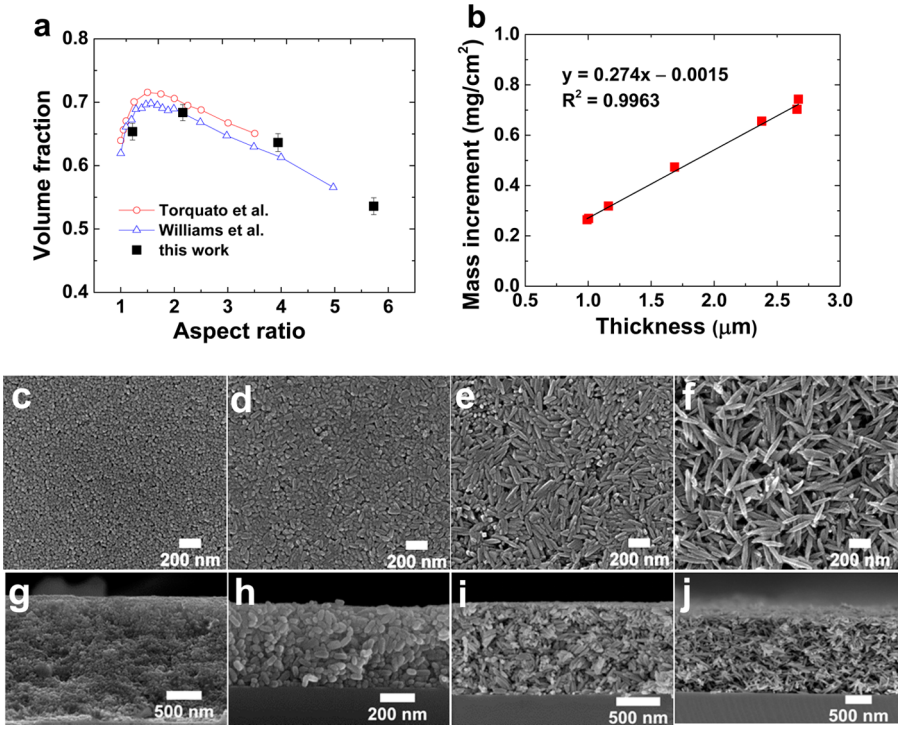


**Figure 1. Structures of disordered $TiO_2$ nanoparticle assemblies. (a) Volume fraction of $TiO_2$ DNAs as a function of AR, compared to theoretical results reported in refs 12 and 13. In panel (a), each point is a statistical average of 5 measurements. The error bars represent the standard error of the means. (b) Mass increment of AR4 DNAs as a function of film thickness. SEM images of ellipsoidal DNAs of (c) and (g) AR1 DNA, (d) and (h) AR2 DNA, (e) and (i) AR4 DNA, and (f) and (j) AR6 DNA. Top: plan-view; bottom: cross-section view.**

nonspherical particles has been extensively studied, albeit mostly using computational methods.[11]

In this work, we investigate the mechanical response of DNAs and present the effect of particle shape anisotropy on their packing and mechanical behaviors. DNAs made of nanoscale prolate ellipsoids with different aspect ratios (AR) are generated, and their mechanical properties are studied using nanoindentation. We show that high aspect ratio nanoellipsoids toughen DNAs and suppress the formation of shear bands, which likely is associated with the brittleness of DNAs. Our results indicate that particle shape anisotropy is a novel design strategy to impart toughness to DNAs without compromising their stiffness and hardness and could potentially be used to generate tough and ductile disordered systems of different length scales.

## RESULTS AND DISCUSSION

We investigate the effect of particle shape anisotropy on the mechanical behavior of DNAs by using prolate nanoellipsoids with various aspect ratios. Each DNA is prepared by spin coating a suspension of $TiO_2$ nanoellipsoids onto a Si substrate. DNAs of nanoellipsoids with aspect ratio (AR) of about 1, 2, 4, and 6 are used and denoted as AR1, AR2, AR4 and AR6 DNA, respectively. Figure 1a shows that the volume fraction of these DNAs, determined using gravimetric analysis, depends on the AR of nanoellipsoids. The volume fraction of DNAs changes nonmonotonically as a function of AR; AR2 DNA has the highest packing fraction of 0.68, whereas AR6 DNA has the lowest (0.54). Interestingly, AR1 and AR4 DNAs have an essentially identical volume fraction (0.65), enabling us to study the effect of particle shape anisotropy without the influence of different packing fractions. The volume fraction of these DNAs is independent of their thicknesses (Figure 1b), which suggests that, within the range of thicknesses investigated here, the packing of nanoellipsoids is not significantly influenced by the presence of the film surface and the film–substrate interface. The experimentally measured packing fractions are in excellent agreement with previous theoretical results on the packings of prolate spheroids (Figure 1a).[12,13]

The plan-view and cross-sectional scanning electron microscopy (SEM) images of DNAs show the random packings of nanoparticles in these films (Figure 1c–j). In fact, some nanoellipsoids throughout the film thickness in AR2, AR4, and AR6 DNAs have out-of-plane, even perpendicular, orientations. The two-dimensional order parameter $P$ of AR2, AR4, and AR6 DNAs ($P = \sum_{i=1}^{N} (\cos 2\theta_i)/N$, where $\theta_i$ is the angle of particle $i$ relative to the local director, and $N$ is the number of ellipsoids in each SEM image), determined from the top and cross-section surfaces,[14] are 0.11, 0.15, and 0.08, respectively. These results confirm that DNAs are essentially randomly structured without preferred orientation, compared to typical liquid crystal materials ($P \sim 0.7$–$0.8$).[15]

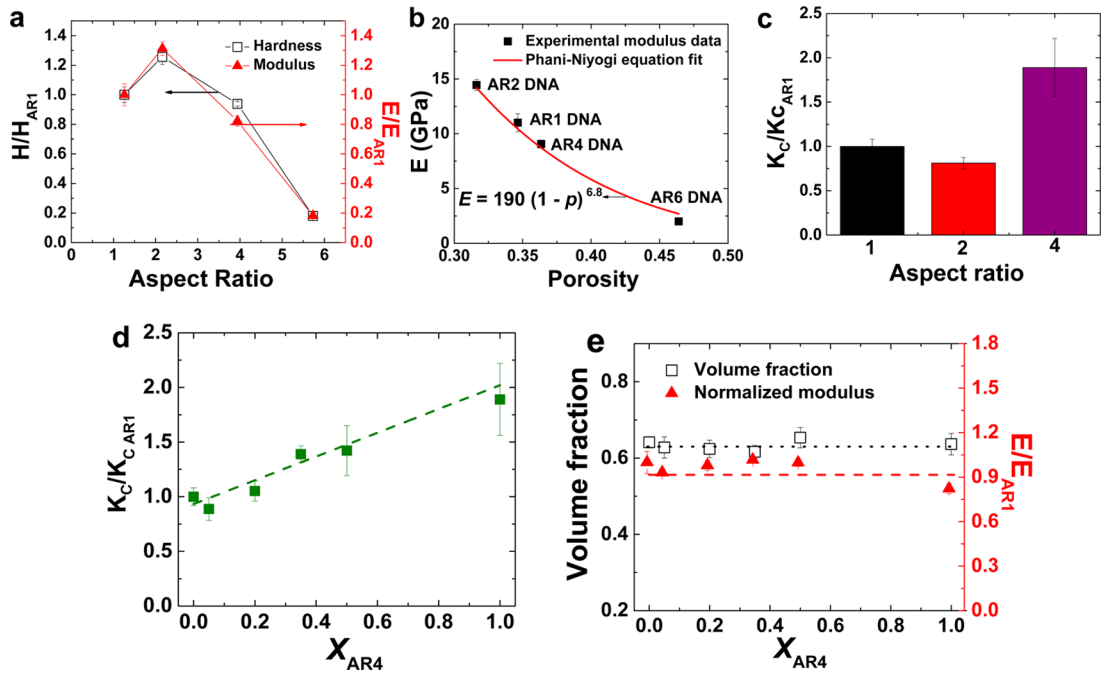


**Figure 2. Mechanical properties of DNAs based on indentations using a *Berkovich* indenter. (a) Hardness ($H$) and modulus ($E$) as a function of AR, (b) Phani−Niyogi equation fit to the modulus-porosity data, and (c) fracture toughness ($K_c$) vs. AR. (d) Fracture toughness ($K_c$) and (e) volume fraction and modulus of AR4-doped AR1 DNAs as a function of volume fraction of AR4 ellipsoids in AR1 DNA ($X_{AR4}$). The hardness, modulus, and fracture toughness are normalized with respect to the absolute values of AR1 DNA ($H_{AR1}$ = 0.23 ± 0.01 GPa, $E_{AR1}$ = 11.01 ± 0.61 GPa, and $K_{C,AR1}$ = 0.032 ± 0.002 MPa·m$^{1/2}$). The error bars shown represent the standard deviation of the arithmetic means. The thicknesses of the films used for the mechanical characterization are ~6 $\mu$m.**

We characterize the mechanical properties of these DNAs as a function of AR using nanoindentation and show (in Figure 2a,b) that the modulus $E$ and hardness $H$ depend strongly on the volume fraction but not significantly on AR, as explained below. Each point in Figure 2a is a statistical average of 16 continuous stiffness measurement (CSM) results in the region of $h$ = 500−1500 nm. $H$ represents the material resistance to plastic deformation during indentation and is proportional to the yield strength of the material.[16] The details of the substrate effect correction method used to obtain $E$ is provided in the Supporting Information. We find that the packing fraction, rather than the particle AR, is the dominant factor that determines $E$ and $H$ of DNAs. AR2 DNA exhibits the highest $E$ and $H$, whereas AR6 DNA has the lowest values. Interestingly, AR1 and AR4 DNAs have approximately the same $E$ and $H$ (Figure 2a), indicating that the packing fraction, rather than the particle AR, is the dominant factor that determines modulus and hardness.

We use a semiempirical model eq 1[17] that has been widely used to describe the modulus of porous solids to reveal the porosity dependence of Young's modulus of DNAs:

$$E = E_0(1 - ap)^n \quad (1)$$

where $E$ and $E_0$ are the Young's moduli at porosity $p$ and zero, respectively. $a$ and $n$ are parameters that provide information about the morphology and pore structure of the material. Within the porosity range of our DNAs, the modulus-porosity data show an excellent fit to eq 1 with $a$ = 1 and $n$ = 6.8 (Figure 2b). The fitted value for $E_0$ (190 GPa) is in good agreement with the reported Young's modulus for bulk $TiO_2$ (178 ± 1 GPa).[18] The value for $n$ (6.8) indicates that the pores in DNAs are nonspherical and interconnected, consistent with the morphology of the DNAs.[17]

While the modulus and hardness are important material properties, they are insufficient to capture the full mechanical behavior of DNAs. The resistance of a material to fracture, quantified in terms of fracture toughness $K_c$, is one of the most important physical properties that determine the damage tolerance of a material. We analyze the indentation-induced cracks in DNAs (Supporting Information Figure S1) to calculate the fracture toughness of DNAs using the following:[19]

$$K_c = \alpha\sqrt{\frac{EP_{max}}{Hc^{3/2}}} \quad (2)$$

where $E$ and $H$ are the nanoindentation-determined modulus and hardness of the film, $P_{max}$ is the maximum indentation load, $c$ is the radial crack length, and $\alpha$ is a prefactor dependent on the indenter geometry (0.016 for Berkovich indenter[19]). Eq 2 has been widely used to determine the fracture toughness through analyzing indentation-induced cracks for a wide range of materials.[20−22] Figure 2c shows that AR2 DNA has the lowest $K_c$, which is expected as stiffer and harder materials tend to be more brittle.[23] Interestingly,

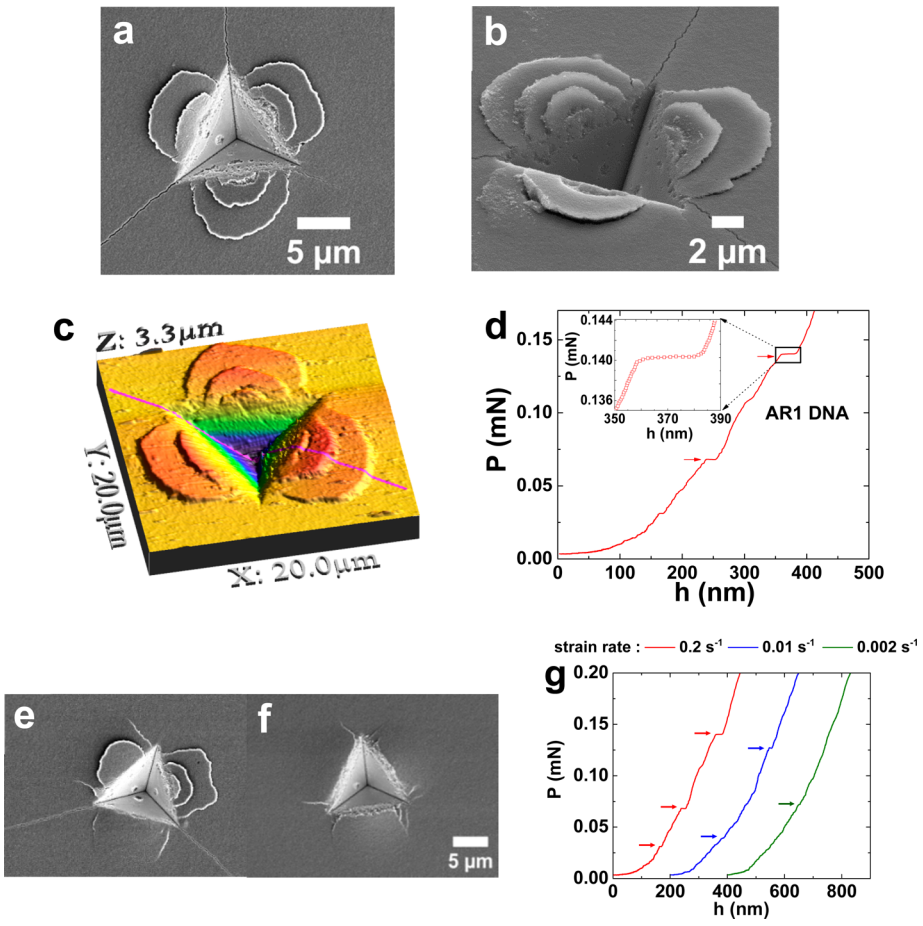


**Figure 3. Effect of strain rate on the shear band formation in *AR1* DNAs based on indentations using a *cube-corner* indenter. (a) SEM image of an indent at a strain rate of 0.2 $s^{-1}$. (b) SEM image of an indent at strain rate of 0.2 $s^{-1}$. The image is taken at an angle of 52°. (c) 3D image of AFM topography of an indent at a loading rate of 250 $\mu Ns^{-1}$. (d) *P*−*h* curve during a nanoindentation at a strain rate of 0.2 $s^{-1}$; the inset shows a magnified plot of a displacement burst. SEM images of indents at (e) 0.01 $s^{-1}$ and (f) 0.002 $s^{-1}$. (g) *P*−*h* curves during indentations at strain rates of 0.2, 0.01, and 0.002 $s^{-1}$. The origin of each curve in (g) has been offset for clear viewing, and several pop-in events have been denoted by arrowheads. Also, see effects of strain rate and loading rate on the shear band formation in AR1 and AR2 DNAs in Supporting Information Figures S2−S4. The thicknesses of the films used for the mechanical characterization are ~6 $\mu$m.**

however, AR4 DNA exhibits much higher, almost 2-fold, fracture toughness than AR1 DNA (Figure 2c), despite the comparable hardness and modulus.

We test whether AR4 nanoellipsoids can be used as "dopants" to toughen AR1 DNAs without sacrificing the strength. Figure 2d clearly shows that the fracture toughness of the AR1−AR4 "blend" DNAs increases linearly, up to a factor of 2, with the concentration of AR4 nanoellipsoids, while the volume fraction, thus *E* and *H*, remain constant (Figure 2e and Supporting Information Figure S10f). It is interesting to note that our finding on the constant packing fraction of these blend films is in excellent agreement with a recent report based on granular packings of AR1 sphere and AR4 spherocylinder (particles of mm scale), which showed that the packing fraction of such mixtures is compositionally independent.[24] Remarkably, AR6 DNAs show no cracks (Supporting Information Figure S1), indicating high fracture toughness. These toughness results clearly indicate that using *high* AR ellipsoids can effectively enhance the resistance of DNAs to fracture and, in turn, enhance the fracture toughness of DNAs without sacrificing the stiffness and hardness (i.e., strength). More importantly, these toughness results clearly indicate that DNAs are a unique class of porous materials in the sense that there is no trade-off between the strength and toughness, which is observed in typical porous solids.

While nanoindentation using a Berkovich tip reveals the effect of particle anisotropy on the mechanical properties of the DNAs, we find that nanoindentation using a *cube-corner* tip provides fundamental insights into the origin of the brittleness of *small* AR DNAs and also the enhanced fracture resistance of *high* AR DNAs. The features associated with nanoindentation of AR1 DNAs using the cube-corner tip strikingly resemble the shear bands that have been observed in nanoindented metallic glasses (MGs), which are amorphous materials made of "disordered packings" of atoms.[25] Circular patterns form around each indent (Figure 3a−c) and

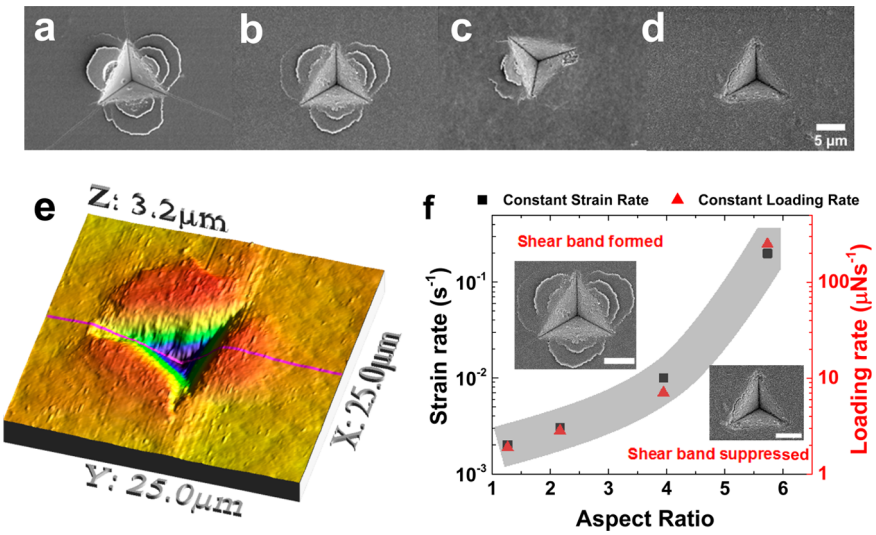


**Figure 4. High AR ellipsoids are effective in suppressing shear band formation in DNAs. SEM images of cube-corner indents in (a) AR1 DNA, (b) AR2 DNA, (c) AR4 DNA, and (d) AR6 DNA at a strain rate of 0.2 $s^{-1}$. Also, see shear band suppression in AR6 DNA upon indentation at various strain and loading rates in Supporting Information Figures S7–S9. (e) 3D AFM topography of an indent by a cube-corner tip in AR4 DNA at a loading rate of 250 $\mu Ns^{-1}$. (f) Deformation state diagram illustrating the effect of deformation rate and particle AR on the formation/suppression of shear bands. The area under the gray band represents the condition under which shear band formation is completely suppressed. Scale bars in the inset SEM images are 5 $\mu$m. The thicknesses of the films used for mechanical characterization are ~6 $\mu$m.**

protrude from the film surface with a step-like morphology, as seen in the atomic force microscopy image (Figure 3c).[26−28] Also, discrete displacement bursts are observed in the load−displacement curves, which indicate sudden penetrations of the indenter into the DNAs at a fixed load (Figure 3d and Supporting Information Figure S2). The extent of shear bands becomes less pronounced with decreasing strain rates as seen in Figure 3a,e,f, and, accordingly, the serrations in the load−displacement curves disappear with decreasing deformation rate (Figure 3g). These observations are hallmarks of shear band formation in nanoindented MGs. Nanoindentation of AR2 DNAs also shows similar trends (Supporting Information Figures S3 and S4).

It is interesting to see such strong strain-rate dependence in shear band formation, which indicates that the deformation of DNAs, i.e., the rearrangement in disordered DNAs, is rate-dependent. This rate-dependent behavior suggests that the sliding between nanoparticles under the applied stress may be a thermally activated process and needs time to overcome the weak interaction energy barrier. Recent experiments involving single-asperity friction have revealed rate dependency and indicated that friction at the nanoscale is a thermally activated process.[29−31] It is plausible that this rate dependence may diminish in disordered assemblies composed of larger particles because of the reduced surface-to-volume ratio. The particle size dependence of the mechanical response of disordered assemblies (e.g., rate dependence) warrants future investigation.

Shear bands are narrow zones of concentrated shear strain, which are thought to be the precursors of brittle fracture in amorphous materials such as MGs and granular packings.[25,32] To our best knowledge, our results are the *first* observation of shear band formation in the assemblies of disordered nanoparticles. More importantly, our results on shear band formation in DNAs suggest a commonality between the deformation behaviors of the two disordered solids with different constituent length scales: MGs and DNAs. It is generally accepted that collective atomic rearrangements called shear transformation zones (STZ), each of which is highly localized within ~20 atoms in width, are the fundamental plasticity carriers in MGs, and their spatiotemporal distribution under applied stress determines the deformation mode. Shear bands form when STZs spontaneously localize within a narrow region and instantly propagate above a critical stress.[33] The propagation of shear bands subsequently leads to catastrophic failure such as brittle fracture in MGs. We believe a similar mechanism is responsible for the development of shear bands in DNAs. When a cube-corner tip, which is known to generate a greater shear stress than the Berkovich tip for a given load/displacement,[16,34] imposes severe stress that exceeds the yield stress of a DNA, shear bands initiate and propagate because of strain localization. Thus, we attribute the brittleness of small AR DNAs to an analogous mechanism that accounts for the brittleness of MGs.

We seek to understand the toughening mechanism of high AR nanoellipsoid-containing DNAs by studying shear band formation. Remarkably, at a given indentation rate, shear band severity indeed decreases with increasing the AR of DNAs (Figure 4a−d, and Supporting Information Figures S5−S9). In fact, shear band formation in AR6 DNAs is completely suppressed

(Figure 4d and Supporting Information Figures S7−S9), and, correspondingly, the serrations are not observed in the load−displacement curves (Supporting Information Figures S8 and S9). Figure 4e shows the indent topography in AR4 DNA with smooth pile-ups, a hallmark of ductile materials.[35] Consistent with the toughening observed in AR4 nanoellipsoid-doped AR1 DNAs, adding a small amount of AR4 nanoellipsoids into AR1 DNA significantly suppresses shear band formation (Supporting Information Figure S10a,b). With a further increase in the fraction of AR4 nanoellipsoids, we see the complete suppression of shear bands (Supporting Information Figure S10c,d) and hence smooth loading curves (Supporting Information Figure S10e).

We also find that DNAs with higher AR nanoellipsoids are able to suppress shear bands at higher deformation rates, as indicated in Figure 3a,e−g, and Supporting Information Figures S2−S5. The effect of particle AR and deformation rate on shear band formation/suppression in the DNAs is summarized as a state diagram (Figure 4f), providing a new design principle for the fabrication of mechanically robust and durable colloidal films for specific applications.

The suppression of shear bands, which leads to the toughening of DNAs with high AR nanoellipsoids, indicates that anisotropic particles are able to hinder and deflect strain localization, resulting in homogeneous deformation, as clearly evidenced by the pile-up formation around an indented region in the AR4 DNA (Figure 4e). The physical mechanism by which high AR ellipsoids suppress shear banding is not known, but the nature of the normal modes of vibration of ellipsoids may provide some insights. In jammed packings of spheres, extended and disordered vibrational modes extend all the way down to zero frequency.[36] The addition of an attractive interaction between the spheres shifts these modes to higher frequency,[37] introducing a small fraction of quasilocalized low frequency modes that are strongly anharmonic,[38] with unusually low energy barriers to rearrangements. As a result, rearrangements are localized.[39] In packings of ellipsoids of high aspect ratio, extended and disordered modes also extend down to zero frequency at the jamming transition.[40] However, since the contact number at the transition is below the isostatic number,[12,41] there are also an extensive number of zero-frequency modes. Attractive interactions, which are present in our nanoparticle packings, shift the modes in this "pressure band"[42] upward in frequency. Because of this band, there are many more strongly anharmonic low-frequency modes compared to the case for sphere packings. As a result, most of these are not quasilocalized. It is therefore plausible that localized failure may be suppressed in packings of high AR ellipsoids, compared to spheres.

## CONCLUSION

Mechanical failure such as brittle fracture has significantly restricted the utilization of colloidal films as well as other disordered materials such as MGs and granular solids in applications requiring high durability and reliability. In this work, we have shown that shear band formation in assemblies of disordered nanoparticles can be significantly suppressed by exploiting the shape anisotropy of the constituent nanoparticles. The high AR ellipsoids (*e.g.*, AR4) make tough DNAs on their own and also are effective in enhancing the fracture toughness of AR1 DNAs (up to a factor of 2) without degrading their stiffness and hardness when these particles are added as dopants. Shape anisotropy provides a strategy to toughen DNAs for a variety of applications that require mechanically durable nanoparticle films such as flexible electronics and biomedical devices. Our results also suggest that tailoring anisotropy in interparticle interactions (*e.g.*, directional bonding) could lead to the enhancement of fracture resistance in other amorphous systems such as MGs and granular solids.

## METHODS

**$TiO_2$ Ellipsoidal Particles Synthesis.** $TiO_2$ ellipsoidal particles with aspect ratios (AR) of 1, 2, 4, and 6 are synthesized using a previously reported hydrothermal method.[43] Dimensions for AR1 particles: the minor axis is $2a = 23 \pm 3$ nm, the major axis is $2b = 29 \pm 4$ nm, AR = $1.26 \pm 0.22$; for AR2 particles: $2a = 29 \pm 4$ nm; $2b = 62 \pm 10$ nm, AR = $2.16 \pm 0.35$; for AR4 particles: $2a = 32 \pm 6$ nm, $2b = 122 \pm 6$ nm, AR = $3.94 \pm 0.86$; for AR6 particles: $2a = 32 \pm 5$ nm, $2b = 181 \pm 33$ nm, AR = $5.73 \pm 0.98$.

**Nanoparticle Assembly Fabrication.** $TiO_2$ nanoparticle assemblies are prepared by a spin coating using a WS-400BZ-6NPP/Lite spin coater from Laurell Technologies Corporation. A $TiO_2$ aqueous suspension is dispensed on an acetone-cleaned Si wafer held tightly on the rotary platform of the spin coater by a vacuum and rotates at a speed of 3000 rpm for 3 min to generate a homogeneous film. The suspension concentration is 40 wt % for AR1 and AR2 DNAs; in the case of AR4 and AR6 DNAs, the suspension concentration is 30 wt %. As for AR1 and AR4 blend films, the suspension concentration is 40 wt %. The concentration of AR4 ellipsoidal particles is adjusted to 5, 20, 35, and 50% of the total volume of AR1 and AR4 particles.

**Volume Fraction Measurement.** The volume fraction of $TiO_2$ DNAs ($V_{DNA}$) is determined using gravimetric analysis. The mass of film ($M_{DNA}$) is determined by measuring the mass difference between a bare Si wafer and the same Si wafer after film deposition; then the volume of the porous film ($V_{DNA,P}$) is obtained using the known density of $TiO_2$ ($\rho_{TiO2}$) ($V_{DNA,P} = M_{DNA}/\rho_{TiO2}$). Because the film deposited around the edges of a Si wafer is inhomogeneous, the edges of the film are cut to obtain the homogeneous part for measurement. By measuring the film width, length, and thickness, the bulk volume of the film is determined ($V_{DNA,B}$). The film volume fraction is obtained by $V_{DNA} = V_{DNA,P}/V_{DNA,B}$. At least four measurements are performed for each film to obtain the statistical average of volume fraction.

**Characterization.** Thickness of DNAs is measured using a Zygo 3100 Interferometer. At least five measurements are performed for each sample to obtain the statistical average value. Scanning electron microscopy is performed using a Hitachi S−4800 to examine the morphology of surface, indentation, and shear bands of DNAs. The topology and height profiles of shear bands

in DNAs are characterized using Agilent 5500 Atomic Force Microscope under contact mode.

The mechanical properties of $TiO_2$ DNAs ($\sim 6\,\mu$m in thickness) are characterized through nanoindentation technique using a Nano Indenter G200 from Agilent Technologies, Inc., with continuous stiffness measurement (CSM). The indenter tip area function is calibrated using fused silica, and a constant modulus $E$ is achieved in the depth range of 5−1500 nm. The indenter is stabilized to achieve a thermal drift rate less than 0.05 nm/s before performing any indentation. A Berkovich indenter tip is used to perform to the indentation depth of 2.5 $\mu$m for determining the hardness, Young's modulus, and fracture toughness, and the loading of constant strain rate of 0.04 $s^{-1}$ is used. The CSM option allows the depth profiles of the mechanical properties to be obtained, and the CSM harmonic displacement (amplitude) is set as 1.5 nm. For each sample, a 4 × 4 array (*i.e.*, 16 indentations) is performed, and the result of each 4 × 4 array is analyzed using Agilent Analyst software to determine the statistical averages of hardness and modulus in the indentation depth range of 500−1500 nm. The modulus measured here is Young's modulus, and the value of Poisson's ratio $v$ (0.18) is assumed. To correct for the substrate effect on the indentation modulus, a previously reported method[44] is used to calculate the modulus, which is valid for indentation depth <50% of the film thickness. The substrate effect is generally insignificant if the indentation depth is less than 30% of the film thickness,[35] therefore, the hardness is calculated directly using the Oliver−Pharr method.[35] The fracture toughness is determined using the reported method *via* the characterization of indentation−induced radial cracks.[19] A cube-corner indenter tip is used to perform indentations to the indentation depth of 4.5 $\mu$m for the characterization of shear band formation. The indentations are performed at constant strain rates of 0.2, 0.1, 0.01, and 0.002 $s^{-1}$ and constant loading rates of 250, 50, 7, and 0.5 $\mu Ns^{-1}$. For each sample, a 3 × 3 array is performed.

*Conflict of Interest:* The authors declare no competing financial interest.

*Acknowledgment.* This work was supported by the PENN MRSEC DMR-1120901 and an NSF CAREER Award (DMR-1055594). G.F. is thankful for the support from a Pennsylvania Keystone Innovation Starter Kit (KISK) grant and also appreciates the technical support from Agilent Technologies, Inc. T.B. acknowledges the graduate fellowship from Fundación "La Caixa". Z.Z. acknowledges the George F. Carrier Fellowship. We thank Professor Daniel Hammer (University of Pennsylvania) for the use of a lyophilizer and Professor Robert Carpick (University of Pennsylvania) for the use of an interferometer. We also thank Professors Daniel Gianola, Robert Carpick, and Arjun Yodh (University of Pennsylvania) for careful reading of our manuscript.

*Supporting Information Available:* SEM images of Berkovich indents on DNAs, SEM images and load−displacement curves of cube-corner indents on AR1 DNA at constant loading rates, SEM images and load−displacement curves of cube-corner indents on AR2, AR4, and AR6 DNAs at constant loading rates and strain rates, the height profile of cube-corner indentation on AR4 DNA, SEM images and load−displacement curves of cube-corner indents on AR1 and AR4 ellipsoids blend films at constant strain rate, and hardness of AR1 and AR4 ellipsoids blend DNAs as a function of volume fraction of AR4 ellipsoids in AR1 DNA are included. This material is available free of charge *via* the Internet at http://pubs.acs.org.

## REFERENCES AND NOTES

1. Oregan, B.; Gratzel, M. A. Low-Cost, High-Efficiency Solar-Cell Based on Dye-Sensitized Colloidal $TiO_2$ Films. *Nature* **1991**, *353*, 737–740.
2. Dang, C.; Lee, J.; Breen, C.; Steckel, J. S.; Coe-Sullivan, S.; Nurmikko, A. Red, Green and Blue Lasing Enabled by Single-Exciton Gain in Colloidal Quantum Dot Films. *Nat. Nanotechnol.* **2012**, *7*, 335–339.
3. Kim, M.-G.; Kanatzidis, M. G.; Facchetti, A.; Marks, T. J. Low-Temperature Fabrication of High-Performance Metal Oxide Thin-Film Electronics *via* Combustion Processing. *Nat. Mater.* **2011**, *10*, 382–388.
4. Nakanishi, H.; Bishop, K. J. M.; Kowalczyk, B.; Nitzan, A.; Weiss, E. A.; Tretiakov, K. V.; Apodaca, M. M.; Klajn, R.; Fraser Stoddart, J.; Grzybowski, B. A. Photoconductance and Inverse Photoconductance in Films of Functionalized Metal Nanoparticles. *Nature* **2009**, *460*, 371–375.
5. Kim, T.-H.; Cho, K.-S.; Lee, E. K.; Lee, S. J.; Chae, J.; Kim, J. W.; Kim, D. H.; Kwon, J.-Y.; Amaratunga, G.; Lee, S. Y.; et al. Full-Colour Quantum Dot Displays Fabricated by Transfer Printing. *Nat. Photonics* **2011**, *5*, 176–182.
6. Maheshwari, V.; Saraf, R. F. High-Resolution Thin-Film Device to Sense Texture by Touch. *Science* **2006**, *312*, 1501–1504.
7. Shevchenko, E. V.; Talapin, D. V.; Kotov, N. A.; O'Brien, S.; Murray, C. B. Structural Diversity in Binary Nanoparticle Superlattices. *Nature* **2006**, *439*, 55–59.
8. Greer, J. R.; Street, R. A. Mechanical Characterization of Solution-Derived Nanoparticle Silver Ink Thin Films. *J. Appl. Phys.* **2007**, *101*, 103529.
9. Lee, D.; Jia, S.; Banerjee, S.; Bevk, J.; Herman, I. P.; Kysar, J. W. Viscoplastic and Granular Behavior in Films of Colloidal Nanocrystals. *Phys. Rev. Lett.* **2007**, *98*, 026103.
10. Ayouch, A.; Dieudonné, X.; Vaudel, G.; Piombini, H.; Vallé, K.; Gusev, V.; Belleville, P.; Ruello, P. Elasticity of An Assembly of Disordered Nanoparticles Interacting *via* either Van Der Waals-Bonded or Covalent-Bonded Coating Layers. *ACS Nano* **2012**, *6*, 10614–10621.
11. Damasceno, P. F.; Engel, M.; Glotzer, S. C. Predictive Self-Assembly of Polyhedra into Complex Structures. *Science* **2012**, *337*, 453–457.
12. Donev, A.; Cisse, I.; Sachs, D.; Variano, E. A.; Stillinger, F. H.; Connelly, R.; Torquato, S.; Chaikin, P. M. Improving the Density of Jammed Disordered Packings using Ellipsoids. *Science* **2004**, *303*, 990–993.
13. Wouterse, A.; Williams, S. R.; Philipse, A. P. Effect of Particle Shape on the Density and Microstructure of Random Packings. *J. Phys.: Condens. Matter* **2007**, *19*, 406215.
14. Hopkins, P. E.; Mittal, M.; Phinney, L. M.; Grillet, A. M.; Furst, E. M. Ultra-Low Thermal Conductivity of Ellipsoidal $TiO_2$ Nanoparticle Films. *Appl. Phys. Lett.* **2011**, *99*, 133106.
15. Tomasik, M. R.; Collings, P. J. Aggregation Behavior and Chromonic Liquid Crystal Phase of a Dye Derived from Naphthalenecarboxylic Acid. *J. Phys. Chem. B* **2008**, *112*, 9883–9889.
16. Johnson, K. L. *Contact Mechanics*; Cambridge University Press: Cambridge, 1987.
17. Phani, K. K.; Niyogi, S. K. Young's Modulus of Porous Brittle Solids. *J. Mater. Sci.* **1987**, *22*, 257–263.
18. Swamy, V.; Dubrovinsky, L. S. Bulk Modulus of Anatase. *J. Phys. Chem. Solids* **2001**, *62*, 673–675.
19. Pharr, G. M. Measurement of Mechanical Properties by Ultra-Low Load Indentation. *Mater. Sci. Eng., A* **1998**, *253*, 151–159.
20. Anstis, G. R.; Chantikul, P.; Lawn, B. R.; Marshall, D. B. A Critical Evaluation of Indentation Techniques for Measuring Fracture Toughness: I, Direct Crack Measurements. *J. Am. Ceram. Soc.* **1981**, *64*, 533–538.
21. Marshall, G. W.; Balooch, M.; Gallagher, R. R.; Gansky, S. A.; Marshall, S. J. Mechanical Properties of the Dentinoenamel Junction: AFM Studies of Nanohardness, Elastic Modulus, and Fracture. *J. Biomed. Mater. Res.* **2001**, *54*, 87–95.
22. Kruzic, J. J.; Kim, D. K.; Koester, K. J.; Ritchie, R. O. Indentation Techniques for Evaluating the Fracture Toughness of Biomaterials and Hard Tissues. *J. Mech. Behav. Biomed. Mater.* **2009**, *2*, 384–395.
23. Zhang, L.; Prosser, J. H.; Feng, G.; Lee, D. Mechanical Properties of Atomic Layer Deposition-Reinforced Nanoparticle Thin Films. *Nanoscale* **2012**, *4*, 6543–6552.
24. Kyrylyuk, A. V.; van de Haar, M. A.; Rossi, L.; Wouterse, A.; Philipse, A. P. Isochoric Ideality in Jammed Random Packings of Non-Spherical Granular Matter. *Soft Matter* **2011**, *7*, 1671–1674.
25. Kim, J. J.; Choi, Y.; Suresh, S.; Argon, A. S. Nanocrystallization during Nanoindentation of A Bulk Amorphous Metal Alloy at Room Temperature. *Science* **2002**, *295*, 654–657.

26. Schuh, C. A.; Nieh, T. G. A Nanoindentation Study of Serrated Flow in Bulk Metallic Glasses. *Acta Mater.* **2003**, *51*, 87–99.
27. Moser, B.; Löffler, J. F.; Michler, J. Discrete Deformation in Amorphous Metals: An *in situ* SEM Indentation Study. *Philos. Mag.* **2006**, *86*, 5715–5728.
28. Jiang, W. H.; Atzmon, M. Rate Dependence of Serrated Flow in A Metallic Glass. *J. Mater. Res.* **2003**, *18*, 755–757.
29. Greiner, C.; Felts, J. R.; Dai, Z.; King, W. P.; Carpick, R. W. Local Nanoscale Heating Modulates Single-Asperity Friction. *Nano Lett.* **2010**, *10*, 4640–4645.
30. Li, Q.; Dong, Y.; Perez, D.; Martini, A.; Carpick, R. W. Speed Dependence of Atomic Stick-Slip Friction in Optimally Matched Experiments and Molecular Dynamics Simulations. *Phys. Rev. Lett.* **2011**, *106*, 126101.
31. Greiner, C.; Felts, J. R.; Dai, Z.; King, W. P.; Carpick, R. W. Controlling Nanoscale Friction through the Competition between Capillary Adsorption and Thermally Activated Sliding. *ACS Nano* **2012**, *6*, 4305–4313.
32. Gravish, N.; Umbanhowar, P. B.; Goldman, D. I. Force and Flow Transition in Plowed Granular Media. *Phys. Rev. Lett.* **2010**, *105*, 128301.
33. Manning, M. L.; Langer, J. S.; Carlson, J. M. Strain Localization in A Shear Transformation Zone Model for Amorphous Solids. *Phys. Rev. E: Stat., Nonlinear, Soft Matter Phys.* **2007**, *76*, 056106.
34. Wang, L.; Song, S, X.; Nieh, T. G. Assessing Plastic Shear Resistance of Bulk Metallic Glasses under Nanoindentation. *Appl. Phys. Lett.* **2008**, *92*, 101925.
35. Oliver, W. C.; Pharr, G. M. An Improved Technique for Determining Hardness and Elastic Modulus using Load and Displacement Sensing Indentation Experiments. *J. Mater. Res.* **1992**, *7*, 1564–1583.
36. Silbert, L. E.; Liu, A. J.; Nagel, S. R. Vibrations and Diverging Length Scales near the Unjamming Transition. *Phys. Rev. Lett.* **2005**, *95*, 098301.
37. Xu, N.; Wyart, M.; Liu, A. J.; Nagel, S. R. Excess Vibrational Modes and the Boson Peak in Model Glasses. *Phys. Rev. Lett.* **2007**, *98*, 175502.
38. Xu, N.; Vitelli, V.; Liu, A. J.; Nagel, S. R. Anharmonicity and Quasi-Localization of the Excess Low-Frequency Vibrations in Jammed Solids. *Europhys. Lett.* **2010**, *90*, 56001.
39. Manning, M. L.; Liu, A. J. Vibrational Modes Identify Soft Spots in a Sheared Disordered Packing. *Phys. Rev. Lett.* **2011**, *107*, 108302.
40. Zeravcic, Z.; Xu, N.; Liu, A. J.; Nagel, S. R.; van Saarloos, W. Excitations of Ellipsoid Packings near Jamming. *Europhys. Lett.* **2009**, *87*, 26001.
41. Donev, A.; Connelly, R.; F. Stillinger, H.; Torquato, S. Underconstrained Jammed Packings of Hard Ellipsoids. *Phys. Rev. E: Stat., Nonlinear, Soft Matter Phys.* **2007**, *75*, 051304.
42. Schreck, C. F.; Mailman, M.; Chakraborty, B.; O'Hern, C. S. Constraints and Vibrations in Static Packings of Ellipsoidal Particles. *Phys. Rev. E: Stat., Nonlinear, Soft Matter Phys.* **2012**, *85*, 061305.
43. Sugimoto, T.; Zhou, X.; Muramatsu, A. Synthesis of Uniform Anatase $TiO_2$ Nanoparticles by Gel-Sol Method: 3. Formation Process and Size Control. *J. Colloid Interface Sci.* **2003**, *259*, 43–52.
44. Hay, J.; Crawford, B. Measuring Substrate-Independent Modulus of Thin Films. *J. Mater. Res.* **2011**, *26*, 727–738.